Elsevier Editorial System(tm) for Earth and Planetary Science Letters
Manuscript Draft

Manuscript Number: EPSL-D-14-00872R1

Title: Partitioning of light lithophile elements during basalt eruptions on Earth and application to Martian shergottites

Article Type: Letters

Keywords: light lithophiles; degassing; basalt; Kilauea; pyroxene; shergottite

Corresponding Author: Dr. Marie Edmonds, BA MA PhD

Corresponding Author's Institution: University of Cambridge

First Author: Marie Edmonds, BA MA PhD

Order of Authors: Marie Edmonds, BA MA PhD

Abstract: An enigmatic record of light lithophile element (LLE) zoning in pyroxenes in basaltic shergottite meteorites, whereby LLE concentrations decrease dramatically from the cores to the rims, has been interpreted as being due to partitioning of LLE into a hydrous vapor during magma ascent to the surface on Mars. These trends are used as evidence that Martian basaltic melts are water-rich (McSween et al., 2001). Lithium and boron are light lithophile elements (LLE) that partition into volcanic minerals and into vapor from silicate melts, making them potential tracers of degassing processes during magma ascent to the surface of Earth and of other planets. While LLE degassing behavior is relatively well understood for silica-rich melts, where water and LLE concentrations are relatively high, very little data exists for LLE abundance, heterogeneity and degassing in basaltic melts. The lack of data hampers interpretation of the trends in the shergottite meteorites. Through a geochemical study of LLE, volatile and trace elements in olivine-hosted melt inclusions from Kilauea Volcano, Hawaii, it can be demonstrated that lithium behaves similarly to the light to middle rare Earth elements during melting, magma mixing and fractionation. Considerable heterogeneity in lithium and boron is inherited from mantle-derived primary melts, which is dominant over the fractionation and degassing signal. Lithium and boron are only very weakly volatile in basaltic melt erupted from Kilauea Volcano, with vapor-melt partition coefficients <0.1. Degassing of LLE is further inhibited at high temperatures. Pyroxene and associated melt inclusion LLE concentrations from a range of volcanoes are used to quantify lithium pyroxene-melt partition coefficients, which correlate negatively with melt H2O content, ranging from 0.13 at low water contents to <0.08 at H2O contents > 4 wt%. The observed terrestrial LLE partitioning behavior is extrapolated to Martian primitive melts through modeling. The zoning observed in the shergottite pyroxenes is only consistent with degassing of LLE from a Martian melt near its liquidus temperature if the vapor-melt partition coefficient was an order of magnitude larger than observed on Earth. The range in LLE and trace elements observed in shergottite pyroxenes are instead consistent with concurrent mixing and fractionation of heterogeneous melts from the mantle.

Partitioning of light lithophile elements during basalt eruptions on Earth and application to Martian shergottites

Marie Edmonds
Department of Earth Sciences, University of Cambridge, Downing Street, Cambridge CB2 3EQ, United Kingdom, me201@cam.ac.uk

Abstract

An enigmatic record of light lithophile element (LLE) zoning in pyroxenes in basaltic shergottite meteorites, whereby LLE concentrations decrease dramatically from the cores to the rims, has been interpreted as being due to partitioning of LLE into a hydrous vapor during magma ascent to the surface on Mars. These trends are used as evidence that Martian basaltic melts are water-rich (McSween et al., 2001). Lithium and boron are light lithophile elements (LLE) that partition into volcanic minerals and into vapor from silicate melts, making them potential tracers of degassing processes during magma ascent to the surface of Earth and of other planets. While LLE degassing behavior is relatively well understood for silica-rich melts, where water and LLE concentrations are relatively high, very little data exists for LLE abundance, heterogeneity and degassing in basaltic melts. The lack of data hampers interpretation of the trends in the shergottite meteorites. Through a geochemical study of LLE, volatile and trace elements in olivine-hosted melt inclusions from Kilauea Volcano, Hawaii, it can be demonstrated that lithium behaves similarly to the light to middle rare Earth elements during melting, magma mixing and fractionation. Considerable heterogeneity in lithium and boron is inherited from mantle-derived primary melts, which is dominant over the fractionation and degassing signal. Lithium and boron are only very weakly volatile in basaltic melt erupted from Kilauea Volcano, with vapor-melt partition coefficients <0.1. Degassing of LLE is further inhibited at high temperatures. Pyroxene and associated melt inclusion LLE concentrations from a range of volcanoes are used to quantify lithium pyroxene-melt partition coefficients, which correlate negatively with melt H_2O content, ranging from 0.13 at low water contents to <0.08 at H_2O contents > 4 wt%. The observed terrestrial LLE partitioning behavior is extrapolated to Martian primitive melts through modeling. The zoning observed in the shergottite pyroxenes is only consistent with degassing of LLE from a Martian melt near its liquidus temperature if the vapor-melt partition coefficient was an order of magnitude larger than observed on Earth. The range in LLE and trace elements observed in shergottite pyroxenes are instead consistent with concurrent mixing and fractionation of heterogeneous melts from the mantle.

Keywords: light lithophiles, degassing, basalt, Kilauea, pyroxene, shergottite
Word count: 4097

1. Introduction

Decreasing light lithophile element (LLE; lithium, boron, beryllium) concentrations in pyroxenes, from core to rim, have been observed in Martian basaltic shergottite meteorites. These trends have been interpreted to be the result of degassing of the LLE into hydrous vapor during magma decompression towards the Martian surface (Herd et al., 2005; Lentz et al., 2004; McSween et al., 2001; Udry and McSween, 2014). These observations have formed a basis for proposing that Martian primary basaltic melts were H_2O-rich (Beck et al., 2004; Lentz et al., 2001; McSween et al., 2001). The role of H_2O during the petrogenesis of Martian magmas has critical implications for understanding hydrogen distribution during planetary accretion, rheological structure of the Martian mantle, for mantle oxidation state, outgassing and climate, as well as for shaping the surface of the planet. It is not yet clear whether degassing is the correct explanation for these trends, as the partitioning of LLE between melt and vapor during magma decompression is not well understood for basaltic melts. There exist a range of alternative explanations: solid state diffusion of LLE through the crystal during late-stage degassing of the carrier liquid; or fractionation of pyroxene accompanying mixing of liquids, each with distinctive trace element and isotopic characteristics. In this paper the behaviour of lithium and boron is compared to other trace elements and volatiles in primitive melts on Earth and the degassing mechanism is explored in detail.

Lithium and boron are present in basaltic magmas in low concentrations. Owing to their low atomic masses, they are volatile and may exsolve from melts during ascent and eruption. Lithium and boron have an affinity for hydrous fluids in evolved silicic systems during late stage degassing (Webster et al., 1996), in differentiates from Piton de la Fournaise (Vlastélic et al., 2011) and in granitic melts coexisting with fluids (Whitworth and Rankin, 1989). Their abundance in the mantle is influenced strongly by the subduction of lithium-rich sediments into the mantle, inducing heterogeneity both in abundance and in isotopic composition (Kobayashi et al., 2004). Lithium and boron are key tracers for understanding arc geochemical cycling, as they behave like volatile elements during devolatilization, partitioning into fluids at high pressures (Moriguti et al., 2004). Lithium and boron partition weakly into minerals crystallizing from silicate melts, such as pyroxene and plagioclase (Herd et al., 2004), which allows for an observable record of melt lithium and boron contents to be preserved in crystals. If lithium and boron were non-volatile, their abundance in minerals from

core to rim in a closed system would increase inversely proportional to the fraction of liquid remaining, for a fixed partition coefficient. Lithium is enriched in the rims of plagioclase and amphiboles from dacitic lava dome rocks from Mount St Helens, inferred to be due to enrichment in the melt shortly before eruption due to the transfer of vapor from depth (Berlo et al., 2004; Kent et al., 2007b). Little is known, in contrast, about the behavior of LLE in water-poor basalts during low-pressure differentiation and degassing. It has been demonstrated that fluid-melt partition coefficients for lithium and boron are >1 for rhyolites (Webster et al., 1996) and <1 for boron in basalts (Hervig et al., 2002), but there is only limited data on the basaltic end member and no data on lithium partitioning into fluids at low pressures and activities of water. Despite this, their dramatic depletion in pyroxenes from core to rim in Martian basaltic shergottite meteorites has been ascribed to their partitioning into hydrous vapour and hence used as evidence for water in Martian melts (Lentz et al., 2004; Lentz et al., 2001; McSween and Stolper, 1978; McSween et al., 2001; Udry and McSween, 2014).

Other published data have potential to cast light onto the problem of whether Martian basaltic melts are water-rich. The lithium isotopic composition of the pyroxenes, and trends in lithium isotopes from core to rim are expected to indicate either a) diffusive loss of lithium from the crystal through solid state diffusion, which has a characteristic large fractionation factor owing to the large mass difference between the two isotopes, with ^{6}Li expected to diffuse faster (Beck et al., 2004) or b) trends in lithium isotopes consistent with fractionation accompanying degassing of lithium from the melt. In fact the isotopic measurements are inconclusive: δ^{7}Li increases from core to rim, with a magnitude not consistent with solid state diffusive loss of lithium (Beck et al., 2004). This trend is consistent with the preference for ^{6}Li in the gas phase during kinetic fractionation of isotopes (Beck et al., 2004), albeit of a lesser magnitude than predicted; but is not consistent with experiments at high pressures (GPa) illustrating chemical (rather than kinetic) fractionation effects, which show that ^{7}Li is preferentially fractionated into the fluid phase (Vlastélic et al., 2011; Wunder et al., 2006). This latter mechanism appears to be the mechanism at work for transferring light lithium into the mantle in subduction zones (Zack et al., 2003). An alternative and equally viable explanation for the lithium isotope trends is concurrent melt mixing (between melts with distinctive lithium isotope composition) and fractionation of pyroxene.

The concentrations in the pyroxenes, and the pyroxene-melt partition coefficient for lithium inferred from experiments of ~0.2 (Herd et al., 2004), suggest that the primary melt would have had >20 ppm, which is far higher than the lithium content of the whole rocks (Herd et al., 2004). Experiments to reproduce the magnesian cores of the pyroxenes in the

shergottites suggest melt water concentrations of ~1.8 wt% H_2O (Dann et al., 2001), although it has been suggested that the melts may have been chlorine-rich instead (Allard et al., 2005). A role for halogens is supported by the fact that most martian hydrous minerals generally have the relevant sites filled with Cl and F instead of H (Patiño Douce and Roden, 2006). Recent studies of nominally anhydrous minerals (Boctor et al., 2003), amphiboles (McCubbin et al., 2010), and apatites (McCubbin et al., 2012; McCubbin et al., 2014) from Martian meteorites suggest that the martian mantle is as hydrous as that of the Earth. In contrast, olivine melt inclusions in shergottites have undegassed D/H signatures and low total H_2O contents, leading to the conclusion that the Martian mantle is much drier than on Earth (Usui et al., 2012) and would therefore produce relatively dry primary melts. Although both "enriched" and "depleted" shergotites exist, they were both derived from parental magmas with water contents of up to 0.3 wt% and the water contents of their mantle sources were probably somewhat similar (McCubbin et al., 2014).

It is not clear that degassing is the correct explanation for the LLE zoning patterns in shergottite pyroxenes, primarily because we have a poor understanding of the behavior of these elements in basaltic volcanic systems. In order to test the hypothesis, an analogous basaltic system on Earth is used here to quantify the LLE heterogeneity inherited from the mantle and the behavior of lithium and boron during magma decompression, fractionation and degassing. Kilauea Volcano, Hawaii, has oft been cited as a terrestrial analogue to Martian basaltic volcanic system, with its "type I" volcanic gas composition (Gerlach and Graeber, 1985) used to estimate the composition of outgassing volatiles on Mars (Craddock and Greeley, 2009). Kilauea basaltic melts have ~0.7 wt% H_2O prior to degassing (Dixon et al., 1991; Edmonds et al., 2014; Wallace, 1998). Kilauean basaltic melt inclusions, which represent "snapshots" of pre-eruptive melt, contain up to 6.6 ppm Li, up to 3.5 ppm B and up to 330 ppm Cl (Sides et al., 2014b). The behavior of volatile species during magma decompression, fractionation and mixing at Kilauea is well understood (Dixon et al., 1991; Edmonds et al., 2014).

Recently, a dataset comprising > 450 olivine-hosted melt inclusion analyses was generated, spanning 25 eruptions over 600 years of eruptive history (for details of the eruptions sampled see (Sides et al., 2014b). This dataset provides a rich resource for understanding the controls on lithium and boron partitioning (not published previously) and degassing in relatively H_2O-poor (relative to arcs) basalts on Earth. Kilauea lavas do not contain phenocrystic pyroxenes and therefore a synchronous study of lithium partitioning into pyroxene is not possible within this system. However, a collection of mafic pyroxenes (augite and enstatite) from Merapi (Indonesia), Karymsky (Russia) and South Soufriere Hills

(Montserrat, Lesser Antilles), were analyzed for lithium and H_2O in pyroxenes and in their melt inclusions. These data allow assessment of apparent lithium partitioning between pyroxenes and melt at a range of pressures and melt compositions. Empirical models are developed to describe the degassing and partitioning behavior of lithium between melt, pyroxene and vapor, which are used to revisit the data from Martian Shergottite meteorites.

2. Methods

Olivine-hosted melt inclusions were analyzed for major (using electron microprobe), trace (using laser ablation ICP-MS) and volatile (using secondary ion mass spectrometry; SIMS) elements. The major, trace and volatile data were corrected for post-entrapment crystallization (PEC) using Petrolog (which in general resulted in <5% addition of olivine) (Danyushevsky and Plechov, 2011) and, excluding the light lithophile element data, have been published previously (Sides et al., 2014b). The PEC corrections assume that the LLE are similarly compatible to hydrogen in olivine (Kent and Rossman, 2002). The Li, H_2O and B concentrations of olivine- and pyroxene-hosted melt inclusions and in pyroxenes were analyzed using a Cameca IMS-4F ion microprobe at the NERC ion probe facility using a O- primary beam with a net energy of ~17 KeV and a 20 μm spot diameter. Positive secondary ions were extracted and accelerated to ~4.5 KeV. NIST glasses were used as standards and repeat analysis indicates a precision of < 10% and accuracy of < 12%. Lithium and boron-free crystals of forsterite and diopside were analysed and count rates were indistinguishable from background after 3 minutes of sputtering. Minimum detection limits, calculated as three standard deviations above the background count rate are ~200 ppb for boron and ~25 ppb for lithium. The major element composition of the pyroxenes, minerals and glass were analysed using the Cameca electron microprobe at the university of Cambridge. Pyroxene major element composition was analysed with a 15 kV, 10 nA beam focused to a 2 μm spot. Glasses were analysed using a 15 μm, 15 kV beam with 2–4 nA beam current for major elements, and 10 nA beam for minor elements. Na and Si were analysed first with short counting times in order to reduce migration of alkalis (Blundy and Cashman, 2005; Devine et al., 1995; Humphreys et al., 2006).

3. Results

3.1. Lithium and boron relative abundance in melt inclusions

The full set of geochemical data (Cl, H_2O, LLE and trace elements) for the olivine-hosted melt inclusions from Kilauea is given in a **supplementary data** file. A matrix showing the Pearson correlation coefficients, r, characterizing the relationships between lithium and boron and a range of trace elements in the melt inclusions is shown in **Fig 1**. Lithium and boron

behave differently to one another and correlate with a different set of elements. Lithium has a correlation coefficient profile most similar to the light to the rare Earth elements Pr, Nd, Yb and Sm. This finding is consistent with previous work which suggests that lithium and Yb are not fractionated from one another during partial melting (Ryan and Langmuir, 1987). Boron, on the other hand, is most similar, in terms of its correlation coefficient profile, to Hf, U and Rb. Lithium does not correlate strongly with any other element. It displays a weak (r=0.55) correlation with Ba. Boron correlates (with r>0.8) positively with U, Hf, Rb, Zr and negatively (r<-0.8) with Sc, Ti, V and Sr. A plot of lithium versus Yb (**Fig 2**) shows that Kilauea Li/Yb ratios extend to lower and higher values than for MORB (data from (Jenner and O'Neill, 2012)), which are typified by a Li/Yb of ~ 1.7. Previous work has suggested that ocean islands have a Li/Yb > 1.7, based on analyses of whole rock basalts from Pribilof Islands and Kilauea (marked on **Fig 2b**) (Ryan and Langmuir, 1987).

The abundances of lithium and boron in melt inclusions hosted by olivine in basalts worldwide from the Georoc database (which happen to be only from arc settings), are shown in **Fig 3**, along with the Kilauea data from this work. The data show that the Kilauea melts inhabit the high Mg, low water part of the global dataset. Their abundances, at first glance, appear tightly controlled by fractionation with little degassing and little enrichment due to vapor transport, which has been shown to be important for some of the more water-rich, evolved melts (Kent et al., 2007a; Rowe et al., 2008). It is exactly this part of the compositional space and LLE spectrum of behaviors that is relevant for the Martian melts that formed the shergottite meteorites.

3.2. Lithium and boron behavior in basaltic melts during differentiation and degassing

Melt inclusions are hosted by olivines with a range in forsterite (Fo) content from 78 to 89 mol% (**Fig 4**). Kilauea melts are subject to olivine-only fractionation (vectors marked on **Fig 4**) to melt MgO contents of ~ 7 wt%, or olivine Fo contents of ~ 82 mol%. The concentrations of incompatible elements such as Ce in the inclusions span a range of >120% at a fixed olivine forsterite content. The melt inclusions with the highest LREE concentrations are also those with the highest Nb/Y, which ranges from 0.3 to 1.0 (**Fig 4a**) and cannot be explained by olivine fractionation. These relationships indicate that the sample set includes both enriched and depleted melts which reflect either a range in the degree of partial melting, and/or a range in mantle source composition, consistent with recent work (Pietruszka and Garcia, 1999; Sides et al., 2014b). Chlorine concentrations reach 500 ppm in melt inclusions and in general decrease with Fo content, consistent with degassing occurring in tandem with fractionation (**Fig 4b**). Lithium concentrations range from 1.0 to 6.6 ppm in the melt inclusions (**Fig 4c**) and 2.6 to 6.4 ppm in the matrix glasses. Lithium concentrations increase

broadly with decreasing Fo content, consistent with fractionation (**Fig 4c**), but there is a significant range in lithium at a fixed Fo, consistent with heterogeneity inherited from the mantle. The H_2O content of the melt inclusions exhibits a broad range (0.2 to 0.7 wt%) across the entire olivine compositional range, indicating both primary melt heterogeneity and variable degrees of degassing and/or hydrogen loss from the melt inclusions (Sides et al., 2014b). Low lithium concentrations generally correspond to low H_2O concentrations in melt inclusions, suggesting that lithium is degassing to some degree, but this degassing is partially obscured by fractionation and melt heterogeneity. The concentrations of B in the melt inclusions exhibits a large vertical range when plotted against host Fo content (**Fig 4d**); neither fractionation nor degassing trends are clear.

3.3. Lithium abundance in pyroxenes and their melt inclusions

While experimental data exist for the partitioning of lithium between melts and pyroxenes (Brenan et al., 1998a), there are few reports of measurements on natural samples from the literature. Pyroxenes in this study are augites and enstatites from the volcanoes Karymsky (Kamchatka, Russia), Merapi (Indonesia) and South Soufriere Hills (Montserrat, West Indies) and have Mg numbers of 72 to 81 (**Tab 1**). H_2O concentrations reach 190 ppm and lithium concentrations range from 1 to 52 ppm. There are no clear correlations between water and lithium concentrations in the pyroxenes or with any of the pyroxene major element concentrations, apart from a weak correlation between lithium concentration and Mg# (with a correlation coefficient of 0.65 for Karymsky pyroxenes; **Tab 1**).

Major, LLE (Li, B by SIMS) and volatile element (H_2O by SIMS and Cl by EPMA) concentrations of the pyroxene-hosted melt inclusions are shown in **Tab 2**. The glass inclusions are rhyolitic to andesitic in composition. The lithium and boron abundances in the glass phase are meuch higher in the melt inclusions than in the pyroxenes, reaching 56.0 ppm lithium and 58.4 ppm B. In general, there is a relationship between lithium and boron concentration and the H_2O concentration in the melt inclusion, unlike the Kilauea case (**Fig 3b**). Lithium and boron decrease non-linearly with H_2O concentration, with much of the decrease occurring at low H_2O concentrations, consistent with partitioning of the LLE into hydrous vapor (**Fig 5a**) and with previous work (Kent et al., 2007b). Again, there are no clear correlations between the LLE and major elements but there is a moderate correlation between lithium and Cl concentrations in the melt inclusions (r=0.47 for the whole dataset). Pyroxene-melt partition coefficients for lithium and boron (the concentration of the element in the pyroxene over the concentration in the melt) may be calculated by linking the concentrations in the host pyroxene with the included melts (**Tab 3**). Partition coefficients are not correlated with pyroxene Mg# or Al_2O_3 content (**Tab 3**), but correlate strongly with melt

H_2O content, with an r value of -0.89 (**Fig 5b**) such that for low melt H_2O contents the partition coefficient is ~0.15 and for melt H_2O contents >4 wt% it is around half that value, at 0.08. Even though there are considerable compositional differences between the melts and the pyroxenes studied and also with regard to the oxidation states of the various systems, this does not appear to influence the partition coefficient, which is most strongly affected by melt H_2O content and therefore vapor pressure (assuming the melts are vapor-saturated). These partition coefficients agree well with experimentally-derived partition coefficients for lithium in pyroxenes of 0.1-0.2 (Brenan et al., 1998a; Herd et al., 2004).

4. Discussion

Trace element abundances in basaltic melts at Kilauea are influenced heavily by the effects of mixing between heterogeneous melts and fractionation. It is clear that light lithophile element abundances are controlled by the same processes, such that the degassing behavior is not easy to quantify. There is considerable heterogeneity in Li/Yb, that cannot be ascribed to fractionation of olivine. A small fraction of this heterogeneity is probably due to degassing and lithium loss (described below), but the observation of a much larger range in Li/Yb than for MORB (Jenner and O'Neill, 2012), extending to higher values, indicates mantle source heterogeneity with regard to lithium, in common with heterogeneity in the Hawaiian plume source in other elements and isotopes (Blichert‐Toft et al., 2003; Hauri, 1996; Marske et al., 2008; Pietruszka and Garcia, 1999). Quantifying the vapor-melt partitioning behavior of lithium and boron using these data requires eliminating the effects of both fractionation and melt heterogeneity.

4.1. Quantifying partitioning of lithium and boron between basaltic melt and vapour

Plots of elemental or molecular ratios show more clearly the effects of degassing by eliminating both the effects of fractionation and mantle-derived heterogeneity (**Fig 6**). Ce/La is effectively constant with H_2O/La, as it is non-volatile (**Fig 6a**). Cl shows a degassing trend, with Cl/La decreasing with H_2O/La (**Fig 6b**), consistent both with observations of HCl gases emitted from Kilauea and previous work on melt inclusion geochemistry (Anderson and Brown, 1993; Edmonds et al., 2014). When color-coded for olivine host forsterite content (related to melt MgO content, which is proportional to temperature (Helz and Thornber, 1987), there is no trend apparent (**Fig 6b**), suggesting that melt temperature does not influence degassing, consistent with experiments (Webster et al., 1999). Lithium and boron, by contrast, show a large range in Li/La and B/La for a fixed H_2O/La (**Fig 6c, d**). If the data were taken at face value without further graphical differentiation they would show a large degree of scatter and could not easily be interpreted. Color-coding for olivine Fo content

however, allows the degassing trends to emerge. Primitive, hot melts (trapped in high-Fo olivines) have a different behavior with respect to LLE to more evolved, cooler melts.

By assuming a starting, “undegassed” melt composition of 0.7 wt% H_2O and 5 ppm lithium, the trends in **Fig 6c** for “hot” and “cool” melts may be used to estimate the range in vapor-melt partition coefficients (concentration of lithium in the vapor over the concentration of lithium in the melt). The trends are consistent with vapor-melt partition coefficients of 0.07 at high H_2O/La to 0.24 at low H_2O/La for “cooler” degassing, corresponding to olivines in equilibrium with melts at a temperature of 1120-1135 °C (using olivine-melt equilibrium relationships and the MgO melt thermometer (Helz and Thornber, 1987)). For the “hot” melts, at a temperature of >1285 °C, the curve may be reproduced by partitioning of lithium into vapor with a vapor-melt partition coefficient of 0.12 at high H_2O/La decreasing to 0.02 at low H_2O/La. Overall the vapor-melt partition coefficient for lithium ranges from 0.02 to 0.24 and 0.014 to 0.5 for B (**Fig 6d**) (the latter value is the cool, low H_2O/La case), with the partition coefficient having a weak temperature-dependence such that vapor-melt partition coefficients are in general higher at low temperatures. This relationship is consistent with an experimental study conducted at 1 GPa, which showed that clinopyroxene-fluid partition coefficients for lithium ranged from 0.07 to 0.61, the highest values associated with the lowest temperatures (800 °C) (Caciagli et al., 2011). For the shergottites, for which liquidus temperatures were 1240-1260 °C (Stolper and McSween Jr, 1979), the lower vapor-melt partition coefficients may be more appropriate. There is no clear relationship between H_2O/La and pressure derived from H_2O-CO_2 saturation (not shown); this is due to both melt heterogeneity inducing variable relationships between degassing and crystallization; and to the effects of post-entrapment crystallization on CO_2 sequestration into a bubble (Sides et al., 2014a).

4.2. Modelling light lithophile element partitioning, application to Martian meteorites

From the preceding results and analysis the following aspects of LLE partitioning behaviour have been determined, which complement existing experimental data (Brenan et al., 1998b; Caciagli et al., 2011; Herd et al., 2004, 2005): (1) the vapor-melt partition coefficient for lithium and boron suitable for water-poor basaltic melts (from the Kilauea olivine-hosted melt inclusion data) and (2) the pyroxene-melt partition coefficient for lithium for a range of melt water contents (from pyroxene and associated melt inclusion datasets from a range of volcanic centres). Using these results it is now possible to establish relistic models for LLE partitioning between melt, vapor and pyroxenes in water-poor basalts. To model the partitioning of lithium and boron into vapor and into crystallizing pyroxenes the following parameterisation (Villemant et al., 2008; Vlastélic et al., 2011) is used, whereby:

$$C^M = C_0^M . F^{(\quad 1)} \qquad (1)$$

where C^M is the concentration of lithium or boron in the melt, C_0^M is the starting concentration of lithium or boron in the melt, prior to degassing and crystallization, F is the fraction of liquid remaining during fractionation and is a ratio relating the vapor-melt partition coefficient to the pyroxene-melt partition coefficient by assuming that the mass of vapor degassed is proportional to the mass of pyroxene crystallized:

$$= \frac{D^{v\ m} + kD^{s\ m}}{k+1} \qquad (2)$$

where $D^{v\ m}$ is the vapor-melt partition coefficient, $D^{s\ m}$ is the crystal-melt partition coefficient and k is a constant equal to the mass of pyroxene crystallized normalized by the mass of vapor produced. In ocean island settings we estimate this value to be ~ 100, but if the two partition coefficients $D^{v\ m}$ and $D^{s\ m}$ are similar then the value of is highly insensitive to k. We assume that the crystallizing phase assemblage is dominated by pyroxene and therefore $D^{s\ m}$ is a maximum; we use 0.1 for lithium (suitable for melt water contents of < 2 wt%; **Fig 5**) and 0.02 for boron (Brenan et al., 1998a). We use three values for $D^{v\ m}$: 0.1, 1 and 5 to compare the models to the natural data. We use a starting melt composition of 50 ppm for lithium and 30 ppm for B, which is far higher than is observed for basaltic melts on Earth (**Fig 2**) but necessary in order to achieve the concentration profiles in the pyroxenes (Herd et al., 2005). In order to compare the model directly to the shergottite data, we plot the lithium and B concentrations against Ti concentrations, modeled using a starting composition of 0.8 wt% for the primary liquid, a bulk $D^{s\ m}$ of 0.05 and a $D^{pyx\ m}$ of 0.22 (Wood and Blundy, 1997).

The results of the modeling are shown in **Fig 7**. The Kilauea case is typified by an average $D^{v\ m}$ of 0.1 (the full range observed in our data is 0.014 to 0.5, as described in section 4.1). The shergottite data from the Shergotty and Zagami meteorite pyroxenes are also shown (Herd et al., 2005). The array of data shows that in order to explain the lithium and boron data in the shergottite pyroxenes $D^{v\ m}$ must be at least one order of magnitude larger than observed for Kilauea, between 1 and 5. More work is required to fully quantify the range in $D^{v\ m}$ for lithium and boron in basaltic melts at low pressures but it appears that on Earth

these elements are only very poorly volatile in basaltic volcanic systems, particularly so for melts at near-liquidus temperatures. It seems unlikely that the LLE zoning observed in the shergottite pyroxenes is dominantly due to lithium degassing into hydrous vapor, unless there are some as yet unrecognized dependence of partitioning on oxidation state or melt or fluid compositions (e.g. chlorine content), which would result in a much higher $D^{v\ m}$ than observed for terrestrial basalts. The anomalies are unlikely to be due to CO_2 fluxing, as observed in carbon-rich systems on Earth (Métrich and Wallace, 2008), as unreasonable fluxes of CO_2 would be necessary to generate the observed LLE partitioning. The large concentration of lithium and boron in melt in equilibrium with the cores of the shergottite pyroxenes are also far higher than observed in basaltic melts on Earth (**Fig 2**). Degassing is also not consistent with the concurrent large decreases in trace element ratios such as Ce/Y observed in the Shergottite pyroxenes from core to rim (McSween et al., 2001). Cerium is non-volatile in basaltic melts at high temperatures (as shown in **Fig 6**) and so these trends cannot be explained by degassing. The correct interpretation of these trends may have important implications for assessment of primary melt heterogeneity and mixing processes in the mantle and crust of Mars.

5. Conclusions

In summary, the behavior of LLE is characterized during melt mixing, fractionation and degassing at Kilauea Volcano, Hawaii, through a study of olivine-hosted melt inclusions. Lithium behaves similarly to the light to middle rare Earth elements (Nd, Pr, Sm, Yb) during mixing and fractionation of olivine, displaying considerable heterogeneity inherited from primary melts from the mantle, with a Li/Yb exhibiting a range from 0.8 to 2.5, although some of the lower values may be biassed by lithium degassing. In these water-poor basaltic melts, the variability due to mantle heterogeneity swamps the signal arising from both fractionation and degassing. This is in contrast to the variability in lithium and boron in more evolved and water-rich melts, which is dominantly due to partitioning into vapor, which is much more extensive. Lithium and boron partition into vapor weakly in basaltic magmas, with an average vapor-melt partition coefficient of 0.1, although this partitioning appears to be inhibited at higher temperatures. Lithium and H_2O abundance in mafic pyroxenes show that lithium pyroxene-melt partition coefficients range from 0.5 to 1.3, consistent with experimental results. A model incorporating these results to data from the shergottite meteorite pyroxenes shows that in order for degassing to be responsible for the trends observed, the vapor-melt partition coefficient for lithium would need to be more than an order of magnitude greater than for the Kilauea volcano case. It would seem likely, therefore, that primary melt heterogeneity and mixing is a more suitable explanation for the trends in LLE and trace elements in shergottite pyroxenes.

ACKNOWLEDGEMENTS

This work was funded by NERC through the Ion Microprobe facility (IMF grants IMF376/0509 and 429/0511).

REFERENCES CITED

Allard, P., Burton, M., Mure, F., 2005. Spectroscopic evidence for a lava fountain driven by previously accumulated magmatic gas. Nature 433, 407-410.

Anderson, A.T., Brown, G.G., 1993. CO2 contents and formation pressures of some Kilauean melt inclusions. American Mineralogist 78, 794-803.

Beck, P., Barrat, J., Chaussidon, M., Gillet, P., Bohn, M., 2004. Li isotopic variations in single pyroxenes from the Northwest Africa 480 shergottite (NWA 480): a record of degassing of Martian magmas? Geochimica et Cosmochimica Acta 68, 2925-2933.

Berlo, K., Blundy, J., Turner, S., Cashman, K., Hawkesworth, C., Black, S., 2004. Geochemical precursors to volcanic activity at Mount St. Helens, USA. Science 306, 1167-1169.

Blichert‐Toft, J., Weis, D., Maerschalk, C., Agranier, A., Albarède, F., 2003. Hawaiian hot spot dynamics as inferred from the Hf and Pb isotope evolution of Mauna Kea volcano. Geochemistry, Geophysics, Geosystems 4.

Blundy, J., Cashman, K., 2005. Rapid decompression-driven crystallization recorded by melt inclusions from Mount St. Helens volcano. Geology 33, 793-796.

Boctor, N., Alexander, C., Wang, J., Hauri, E., 2003. The sources of water in Martian meteorites: Clues from hydrogen isotopes. Geochimica et Cosmochimica Acta 67, 3971-3989.

Brenan, J., Neroda, E., Lundstrom, C., Shaw, H., Ryerson, F., Phinney, D., 1998a. Behaviour of boron, beryllium, and lithium during melting and crystallization: constraints from mineral-melt partitioning experiments. Geochimica et Cosmochimica Acta 62, 2129-2141.

Brenan, J.M., Neroda, E., Lundstrom, C.C., Shaw, H.F., Ryerson, F.J., Phinney, D.L., 1998b. Behaviour of boron, beryllium, and lithium during melting and crystallization: constraints from mineral-melt partitioning experiments. Geochimica et Cosmochimica Acta 62, 2129-2141.

Caciagli, N., Brenan, J., McDonough, W., Phinney, D., 2011. Mineral–fluid partitioning of lithium and implications for slab–mantle interaction. Chemical Geology 280, 384-398.

Craddock, R.A., Greeley, R., 2009. Minimum estimates of the amount and timing of gases released into the martian atmosphere from volcanic eruptions. Icarus 204, 512-526.

Danyushevsky, L.V., Plechov, P., 2011. Petrolog3: Integrated software for modeling crystallization processes. Geochemistry, Geophysics, Geosystems 12, Q07021.

Devine, J.D., Gardner, J.E., Brack, H.P., Layne, G.D., Rutherford, M.J., 1995. Comparison of microanalytical methods for estimating H2O contents of silicic volcanic glasses. American Mineralogist 80, 319-328.

Dixon, J.E., Clague, D.A., Stolper, E.M., 1991. Degassing history of water, sulfur, and carbon in submarine lavas from Kīlauea Volcano, Hawaii. The Journal of Geology, 371-394.

Edmonds, M., Sides, I.R., Maclennan, J., 2014. Insights into mixing, fractionation and degassing of primitive melts at Kīlauea Volcano, Hawai`i. AGU Monograph.

Gerlach, T.M., Graeber, E.J., 1985. Volatile budget of Kīlauea volcano. Nature 313, 273-277.
Hauri, E.H., 1996. Major-element variability in the Hawaiian mantle plume. Nature 382, 415-419.
Helz, R.T., Thornber, C.R., 1987. Geothermometry of Kilauea Iki lava lake, Hawaii. Bull Volcanol 49, 651-668.
Herd, C.D., Treiman, A.H., Mckay, G.A., Shearer, C.K., 2004. The behavior of Li and B during planetary basalt crystallization. American Mineralogist 89, 832-840.
Herd, C.D., Treiman, A.H., Mckay, G.A., Shearer, C.K., 2005. Light lithophile elements in martian basalts: Evaluating the evidence for magmatic water degassing. Geochimica et Cosmochimica Acta 69, 2431-2440.
Hervig, R.L., Moore, G.M., Williams, L.B., Peacock, S.M., Holloway, J.R., Roggensack, K., 2002. Isotopic and elemental partitioning of boron between hydrous fluid and silicate melt. American Mineralogist 87, 769-774.
Humphreys, M.C., Blundy, J.D., Sparks, R.S.J., 2006. Magma evolution and open-system processes at Shiveluch Volcano: insights from phenocryst zoning. Journal of Petrology 47, 2303-2334.
Jenner, F.E., O'Neill, H.S.C., 2012. Analysis of 60 elements in 616 ocean floor basaltic glasses. Geochemistry, Geophysics, Geosystems 13.
Kent, A.J., Blundy, J., Cashman, K.V., Cooper, K.M., Donnelly, C., Pallister, J.S., Reagan, M., Rowe, M.C., Thornber, C.R., 2007a. Vapor transfer prior to the October 2004 eruption of Mount St. Helens, Washington. Geology 35, 231-234.
Kent, A.J., Rossman, G.R., 2002. Hydrogen, lithium, and boron in mantle-derived olivine: the role of coupled substitutions. American Mineralogist 87, 1432-1436.
Kent, A.J.R., Blundy, J., Cashman, K.V., Cooper, K.M., Donnelly, C., Pallister, J.S., Reagan, M., Rowe, M.C., Thornber, C.R., 2007b. Vapor transfer prior to the October 2004 eruption of Mount St. Helens, Washington. Geology 35, 231-234.
Kobayashi, K., Tanaka, R., Moriguti, T., Shimizu, K., Nakamura, E., 2004. Lithium, boron, and lead isotope systematics of glass inclusions in olivines from Hawaiian lavas: evidence for recycled components in the Hawaiian plume. Chemical Geology 212, 143-161.
Lentz, R., McSween Jr, H., Fayek, M., 2004. Light lithophile abundances and isotopic ratios in Shergottites, Lunar and Planetary Institute Science Conference Abstracts, p. 1633.
Lentz, R., McSween Jr, H., Ryan, J., Riciputi, L., 2001. Water in martian magmas: clues from light lithophile elements in shergottite and nakhlite pyroxenes. Geochimica et Cosmochimica Acta 65, 4551-4565.
Marske, J.P., Garcia, M.O., Pietruszka, A.J., Rhodes, J.M., Norman, M.D., 2008. Geochemical Variations during Kīlauea's Puʻu ʻŌʻō Eruption Reveal a Fine-scale Mixture of Mantle Heterogeneities within the Hawaiian Plume. Journal of Petrology 49, 1297-1318.
McCubbin, F.M., Hauri, E.H., Elardo, S.M., Vander Kaaden, K.E., Wang, J., Shearer, C.K., 2012. Hydrous melting of the martian mantle produced both depleted and enriched shergottites. Geology 40, 683-686.
McCubbin, F.M., Shearer, C.K., Burger, P.V., Hauri, E.H., Wang, J., Elardo, S.M., Papike, J.J., 2014. Volatile abundances of coexisting merrillite and apatite in the martian meteorite Shergotty: Implications for merrillite in hydrous magmas. American Mineralogist 99, 1347-1354.

McCubbin, F.M., Smirnov, A., Nekvasil, H., Wang, J., Hauri, E., Lindsley, D.H., 2010. Hydrous magmatism on Mars: A source of water for the surface and subsurface during the Amazonian. Earth and Planetary Science Letters 292, 132-138.
McSween, H., Stolper, E., 1978. Shergottite Meteorites, i: Mineralogy and Petrography, Lunar and Planetary Institute Science Conference Abstracts, pp. 732-734.
McSween, H.Y., Grove, T.L., Lentz, R.C., Dann, J.C., Holzheid, A.H., Riciputi, L.R., Ryan, J.G., 2001. Geochemical evidence for magmatic water within Mars from pyroxenes in the Shergotty meteorite. Nature 409, 487-490.
Métrich, N., Wallace, P.J., 2008. Volatile Abundances in Basaltic Magmas and Their Degassing Paths Tracked by Melt Inclusions. Reviews in Mineralogy and Geochemistry 69, 363-402.
Moriguti, T., Shibata, T., Nakamura, E., 2004. Lithium, boron and lead isotope and trace element systematics of Quaternary basaltic volcanic rocks in northeastern Japan: mineralogical controls on slab-derived fluid composition. Chemical Geology 212, 81-100.
Patiño Douce, A.E., Roden, M., 2006. Apatite as a probe of halogen and water fugacities in the terrestrial planets. Geochimica et Cosmochimica Acta 70, 3173-3196.
Pietruszka, A.J., Garcia, M.O., 1999. A Rapid Fluctuation in the Mantle Source and Melting History of Kīlauea Volcano Inferred from the Geochemistry of its Historical Summit Lavas (1790–1982). Journal of Petrology 40, 1321-1342.
Rowe, M., Kent, A., Thornber, C., 2008. Using amphibole phenocrysts to track vapor transfer during magma crystallization and transport: An example from Mount St. Helens, Washington. Journal of Volcanology and Geothermal Research 178, 593-607.
Ryan, J.G., Langmuir, C.H., 1987. The systematics of lithium abundances in young volcanic rocks. Geochimica et Cosmochimica Acta 51, 1727-1741.
Sides, I., Edmonds, M., Maclennan, J., Houghton, B., Swanson, D., Steele-MacInnis, M., 2014a. Magma mixing and high fountaining during the 1959 Kīlauea Iki eruption, Hawai ‘i. Earth and Planetary Science Letters 400, 102-112.
Sides, I.R., Edmonds, M., Maclennan, J., Swanson, D.A., Houghton, B.F., 2014b. Eruption style at Kīlauea Volcano in Hawai`i linked to primary melt composition Nature Geoscience 7, 464–469.
Stolper, E., McSween Jr, H.Y., 1979. Petrology and origin of the shergottite meteorites. Geochimica et Cosmochimica Acta 43, 1475-1498.
Udry, A., McSween, H., 2014. New Investigations of Lithium Abundances in Shergottite Pyroxenes and Olivines: Potential Evidence for Martian Magmatic Water, Lunar and Planetary Institute Science Conference Abstracts, p. 1973.
Usui, T., Alexander, C.M.D., Wang, J., Simon, J.I., Jones, J.H., 2012. Origin of water and mantle–crust interactions on Mars inferred from hydrogen isotopes and volatile element abundances of olivine-hosted melt inclusions of primitive shergottites. Earth and Planetary Science Letters 357, 119-129.
Villemant, B., Mouatt, J., Michel, A., 2008. Andesitic magma degassing investigated through H< sub> 2</sub> O vapour–melt partitioning of halogens at Soufrière Hills Volcano, Montserrat (Lesser Antilles). Earth and Planetary Science Letters 269, 212-229.
Vlastélic, I., Staudacher, T., Bachelery, P., Télouk, P., Neuville, D., Benbakkar, M., 2011. Lithium isotope fractionation during magma degassing: constraints from silicic differentiates and natural gas condensates from Piton de la Fournaise volcano (Réunion Island). Chemical Geology 284, 26-34.
Wallace, P.J., 1998. Water and partial melting in mantle plumes: Inferences from the dissolved H2O concentrations of Hawaiian basaltic magmas. Geophysical Research Letters 25, 3639-3642.

Webster, J., Kinzler, R., Mathez, E., 1999. Chloride and water solubility in basalt and andesite melts and implications for magmatic degassing. Geochimica et Cosmochimica Acta 63, 729-738.
Webster, J.D., Burt, D.M., Aguillon, R., 1996. Volatile and lithophile trace-element geochemistry of Mexican tin rhyolite magmas deduced from melt inclusions. Geochimica et Cosmochimica Acta 60, 3267-3283.
Whitworth, M.P., Rankin, A.H., 1989. Evolution of fluid phases associated with lithium pegmatites from SE Ireland. Mineral. Mag 53, 271-284.
Wood, B.J., Blundy, J.D., 1997. A predictive model for rare earth element partitioning between clinopyroxene and anhydrous silicate melt. Contr. Mineral. and Petrol. 129, 166-181.
Wunder, B., Meixner, A., Romer, R.L., Heinrich, W., 2006. Temperature-dependent isotopic fractionation of lithium between clinopyroxene and high-pressure hydrous fluids. Contr. Mineral. and Petrol. 151, 112-120.
Zack, T., Tomascak, P.B., Rudnick, R.L., Dalpé, C., McDonough, W.F., 2003. Extremely light Li in orogenic eclogites: the role of isotope fractionation during dehydration in subducted oceanic crust. Earth and Planetary Science Letters 208, 279-290.

Figure and Table captions

Figure 1. Correlation matrix to illustrate the similarity in behavior of the LLE elements lithium and boron to the rare Earth elements and to highlight correlations between elements. Correlation coefficients are Pearson's correlation coefficients, r, ranging from -1 (blue; perfect negative correlation) to +1 (red; perfect positive correlation).

Figure 2. Plots of Yb against lithium for Kilauea olivine-hosted melt inclusions (yellow), a range of ocean floor MORB (Jenner and O'Neill, 2012) (purple) arc olivine-hosted melt inclusions (from Georoc) and Siberian Traps, Etna and Greenland Tertiary Province olivine-hosted melt inclusions (green). Bottom: enlarged section of the plot with Lithium < 10 ppm to show range in Li/Yb ratios. Also plotted are Pribilof Islands and Kilauea data from (Ryan and Langmuir, 1987).

Figure 3. Lithium (yellow) and boron (red) abundances in olivine-hosted melt inclusions from the Georoc database. Top: lithium and boron (ppm) plotted against melt MgO content. Larger circles with same elemental colours represent the olivine-hosted melt inclusion data from Kilauea from this study. Bottom: lithium and boron abundances plotted against melt inclusion water content in wt%.

Figure 4. Geochemistry of melt inclusions: a. cerium (ppm); b. chlorine (wt%); c. lithium (ppm); and d. boron (ppm), plotted against the olivine Fo content (mol%). Data are color-coded for Nb/Y in a and H_2O concentration in b-d.

Figure 5. a) Lithium, boron (ppm) concentrations plotted against water (wt%) concentrations in pyroxene-hosted melt inclusions from a range of mafic volcanic systems, shown in the legend. b) Lithium pyroxene-melt partition coefficients, $D^{pyx\text{-}melt}$ against melt inclusion H_2O contents, color-coded for lithium content. When the very low lithium content melt inclusions are discarded, the partition coefficient correlates negatively with melt inclusion water content with an r value of -0.89.

Figure 6. Degassing trends in melt inclusions. a. Ce/La; b. Cl/La; c. Li/La; and d. B/La plotted against H_2O/La. Data are color-coded for olivine Fo content (mol%).

Figure 7. Modelling LLE partitioning in Martian pyroxenes. a. lithium and b. boron concentrations plotted against Ti concentrations in pyroxenes from the Shergotty and Zagami meteorites (Herd et al., 2005). Black curves show predicted concentrations of lithium and boron for varying vapor-melt partition coefficients.

Table 1. Pyroxene compositions. Sample names indicate volcanic provenance (MER: Merapi volcano, Indonesia; SSH: South Soufriere Hills Volcano, Montserrat; KAR: Karymsky volcano, Kamchatka). Major elements (in wt%) analysed using EPMA. H_2O and lithium (in ppm) concentrations analysed using SIMS. A description of methods is given in the text.

Table 2. Pyroxene-hosted melt inclusion compositions. Sample names indicate volcanic provenance (MER: Merapi volcano, Indonesia; SSH: South Soufriere Hills Volcano, Montserrat; KAR: Karymsky volcano, Kamchatka). Major elements and Cl (in wt%) analysed using EPMA. H_2O (wt%), lithium and boron (ppm) concentrations analysed using SIMS. A description of methods is given in the text.

Table 3. Pyroxene-melt partitioning data for lithium for where linked pyroxene and melt inclusion data are available (from **Tables 1** and **2**). Mg#, Al_2O_3, H_2O and lithium concentrations for the host pyroxene are shown in columns 2, 3, 4, 5. Melt inclusion H_2O, lithium are shown in columns 6, 7. The pyroxene-melt partition coefficient for Li, $D_{Li,\ pyr\text{-}melt}$, is shown in column 8.

***Highlights (for review)**

- Lithium and boron degassing is quantified for ascending degassing basaltic magmas
- These elements are only weakly volatile in water-poor basaltic melts
- Heterogeneity inherited from the mantle accounts for most of their variability
- LLE zoning in Martian pyroxenes is inconsistent with degassing

Figure 1

Click here to download high resolution image

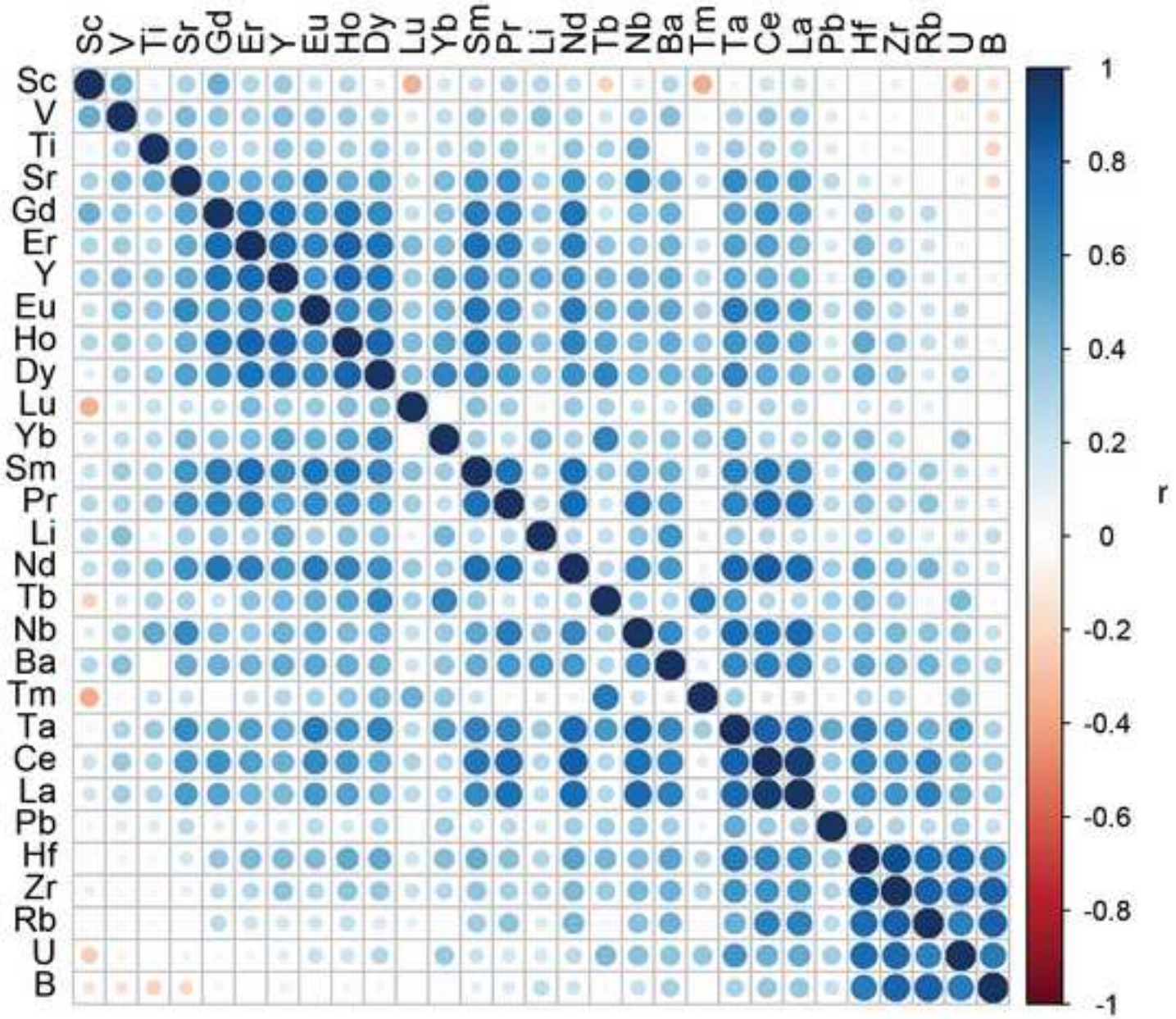

Figure 2
Click here to download Figure: Fig2_Li_Yb_plots.eps

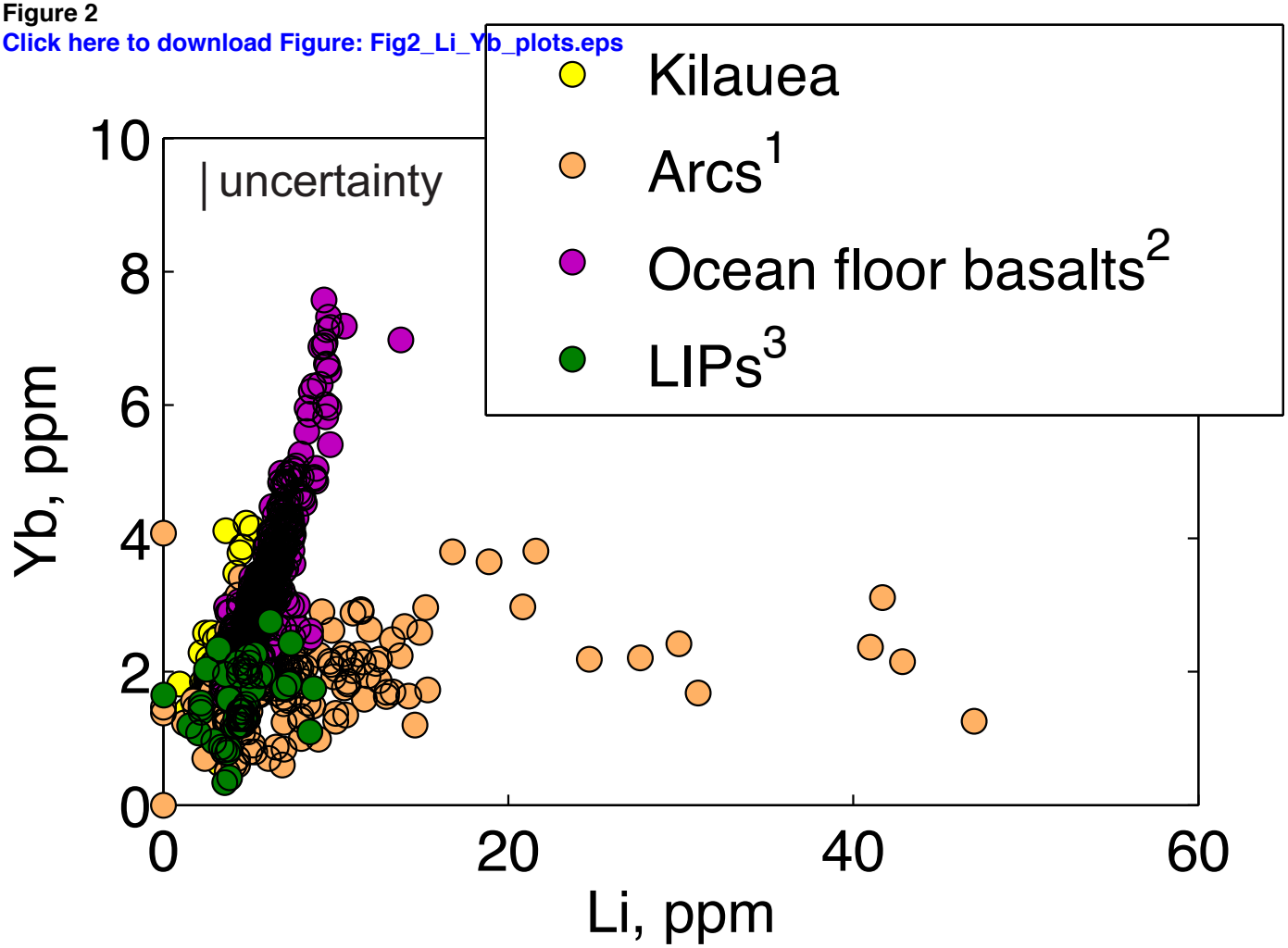

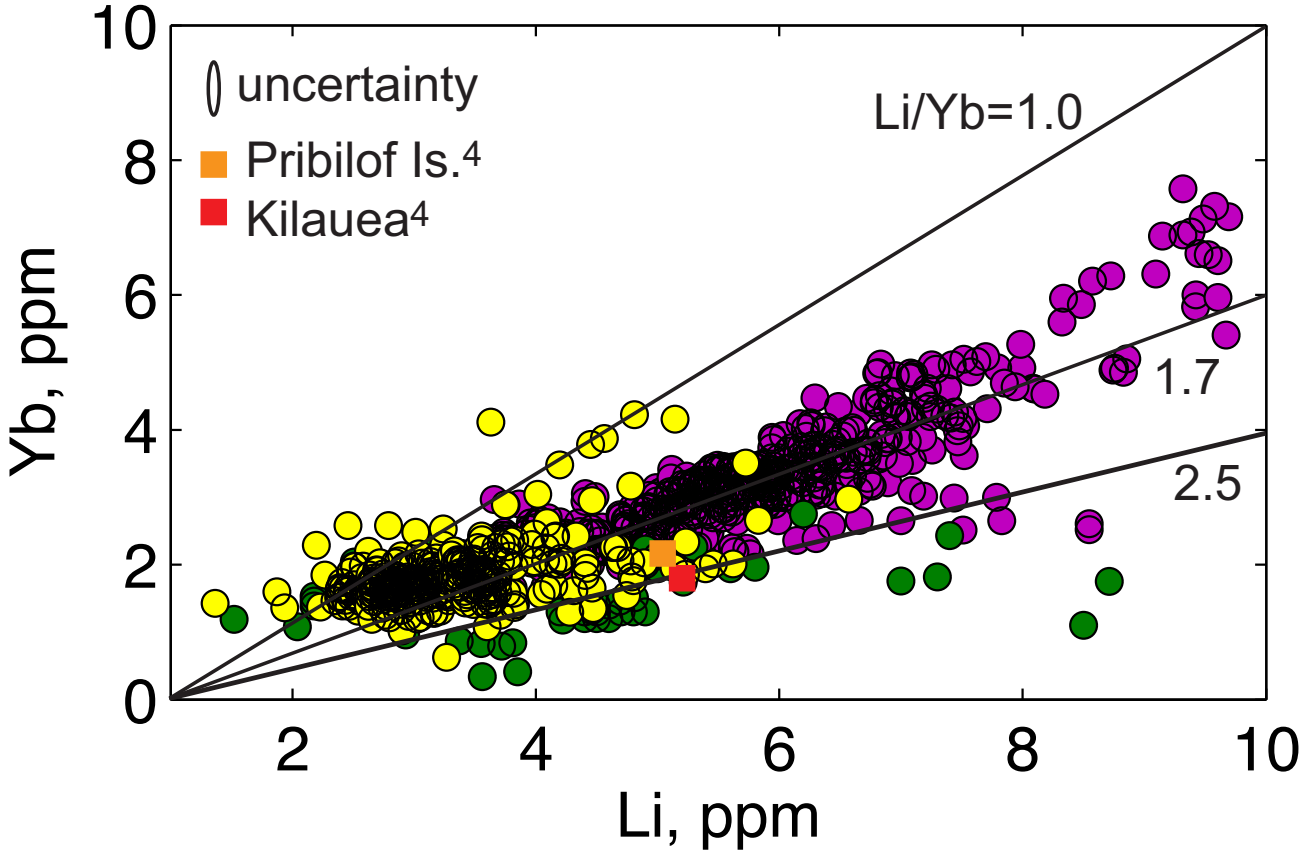

Figure 3
Click here to download Figure: Fig3_globalbasalts_LLE.eps

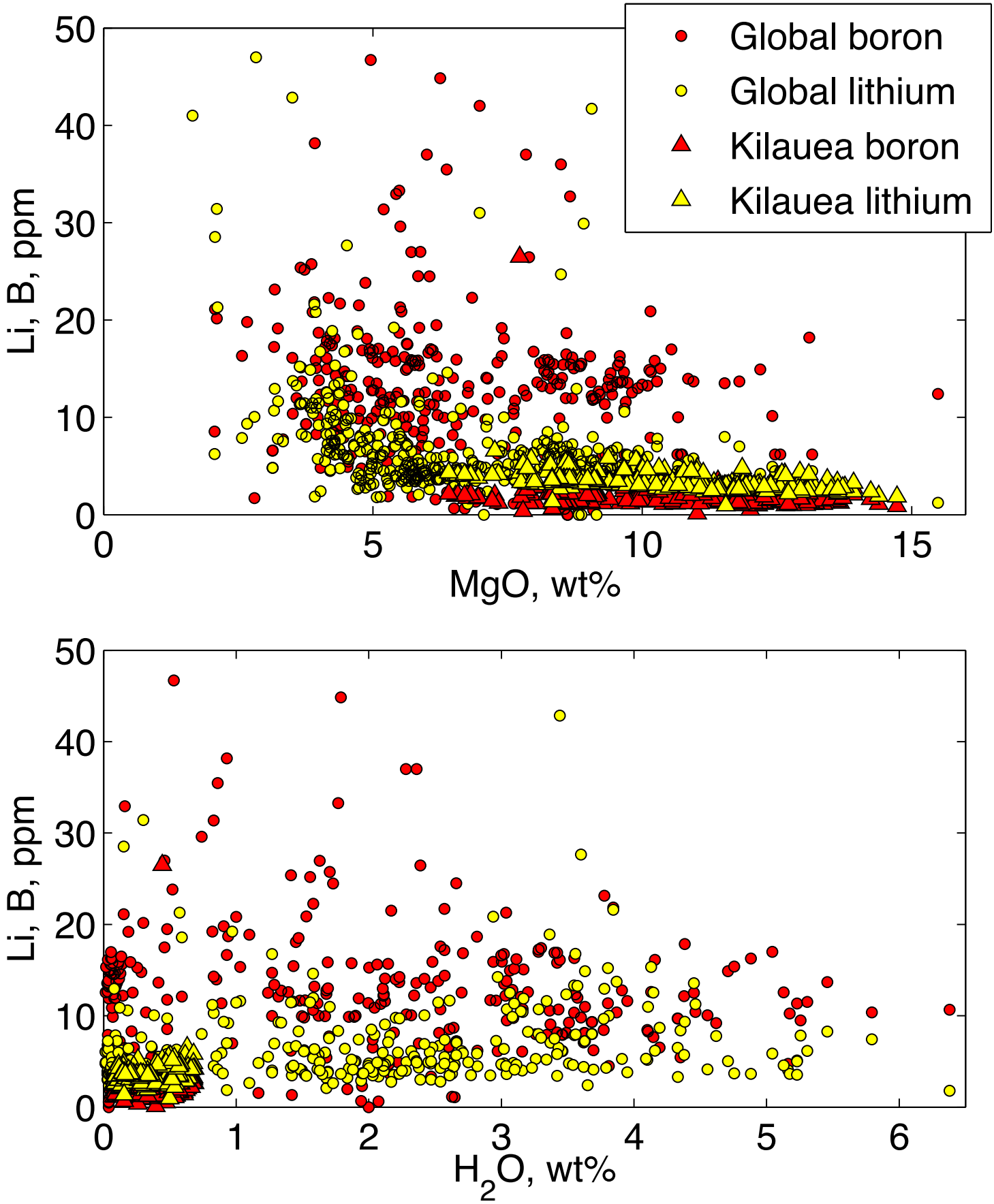

Figure 4

Click here to download Figure: Fig4_data_raw.eps

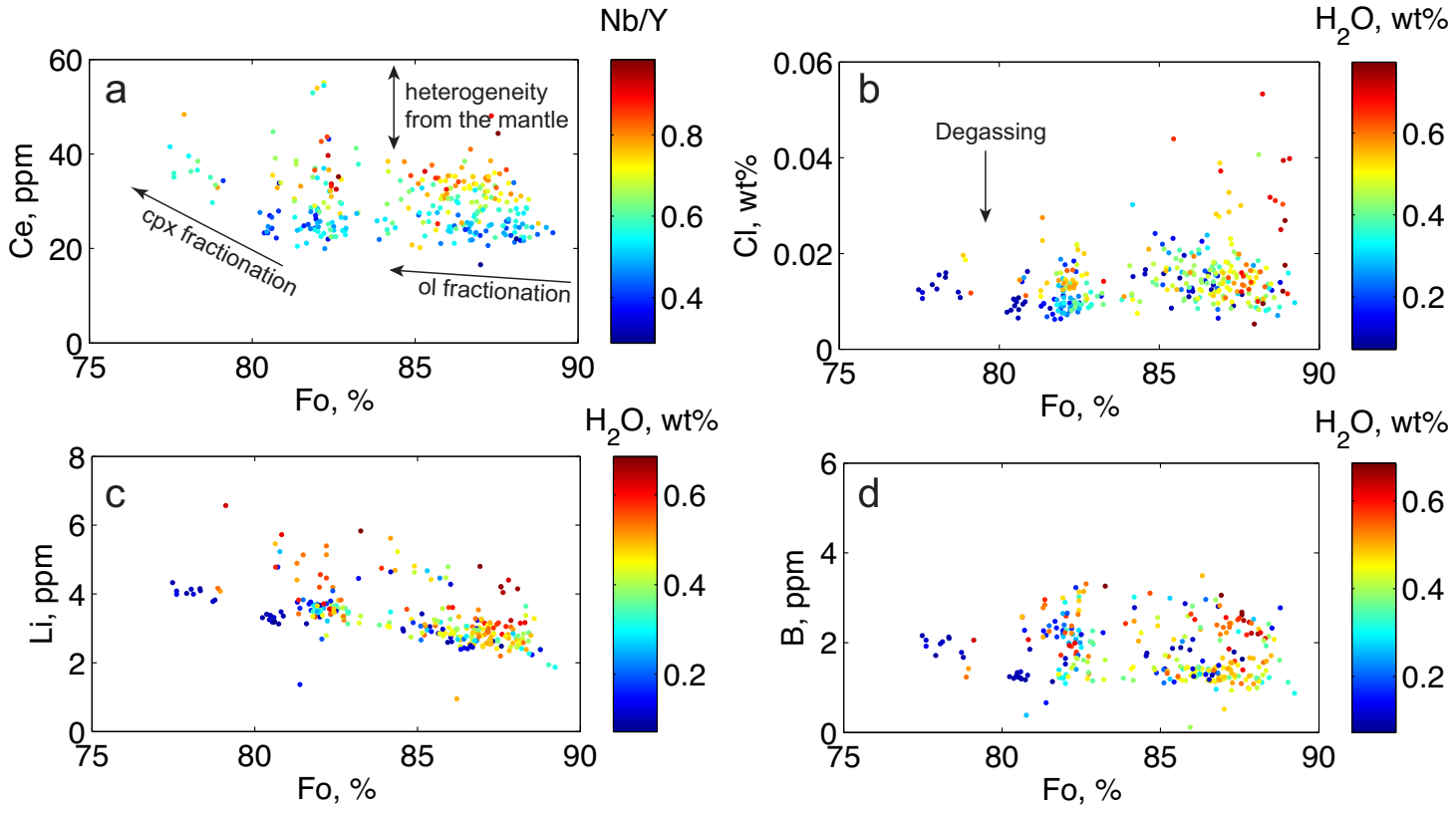

Figure 5
Click here to download Figure: Fig5_pyxdata.eps

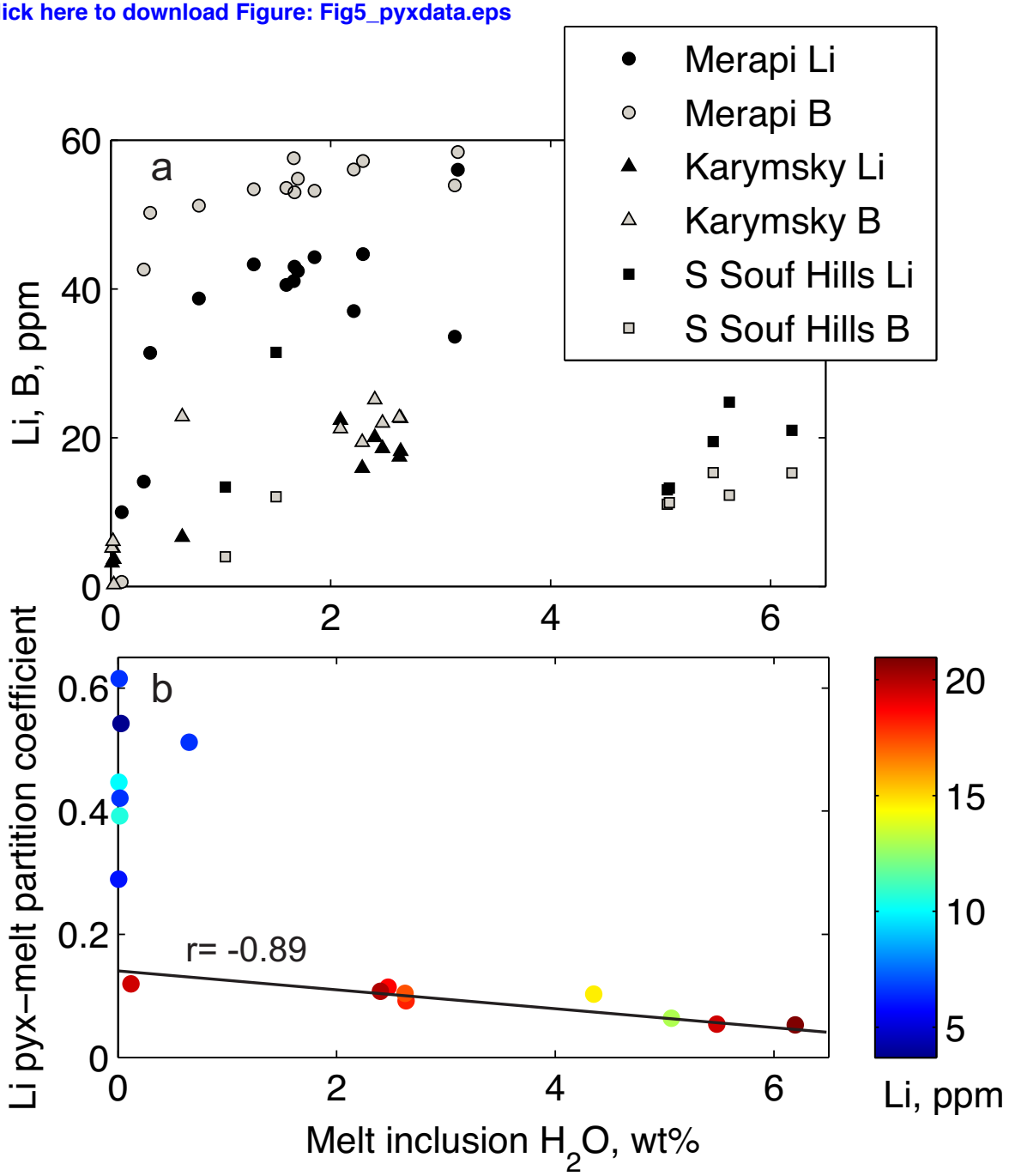

Figure 6

Click here to download Figure: Fig6_data_normalised_Edmonds_figure2.eps

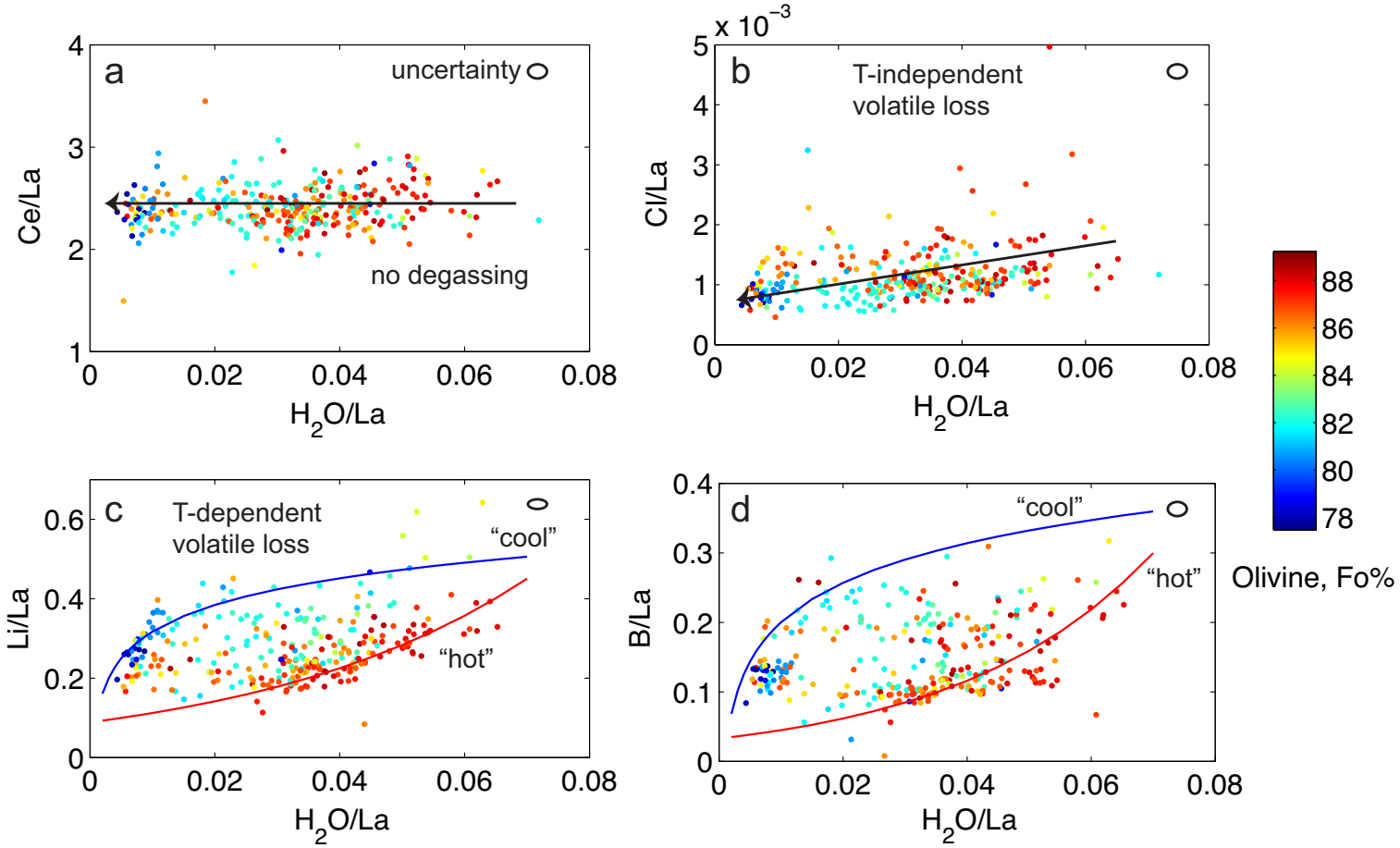

Figure 7
Click here to download Figure: Fig7_Marsdata.eps

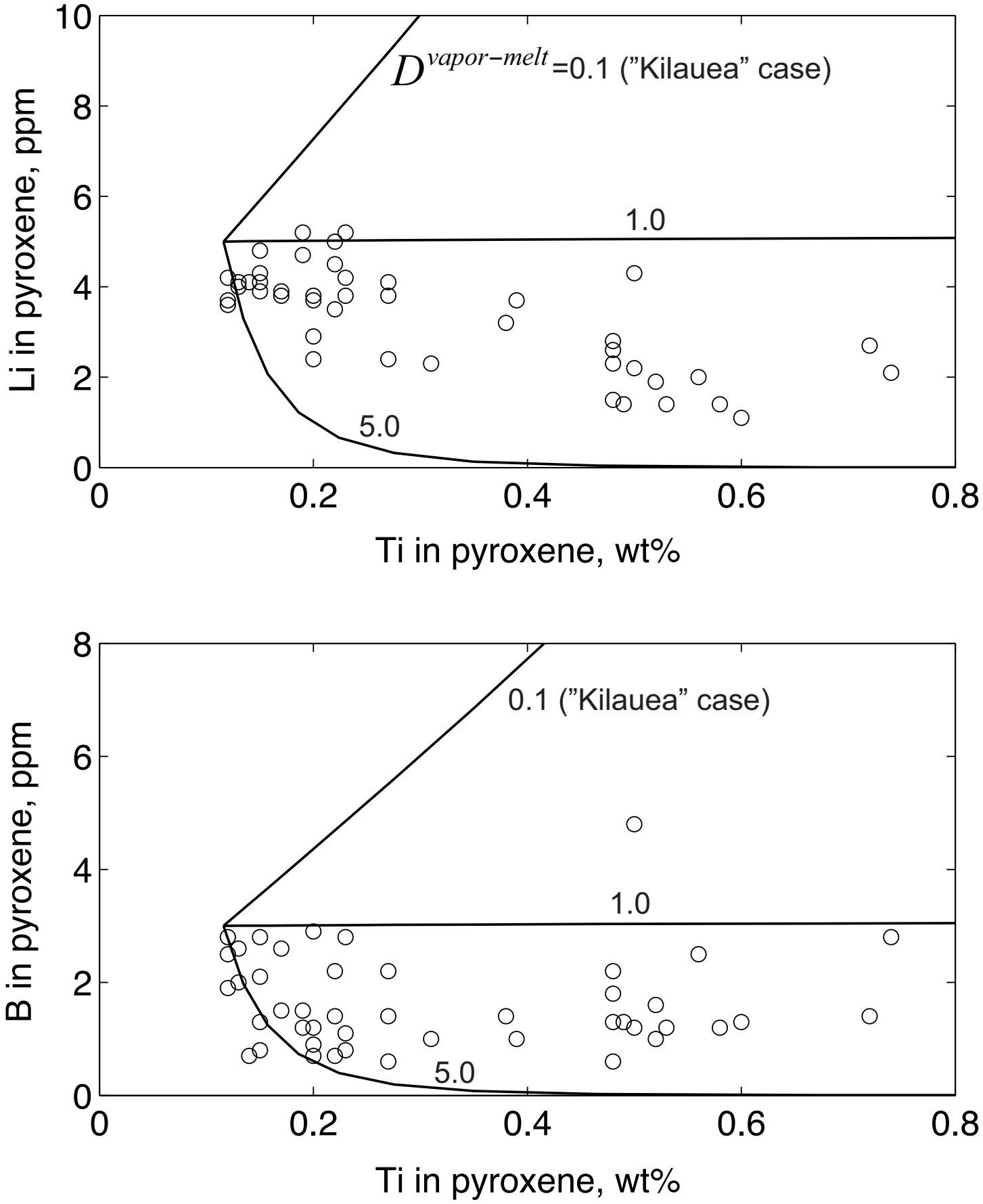

Table 1

Click here to download Table: Tab1_pyxdata.docx

	Na_2O	SiO_2	MgO	Al_2O_3	K_2O	CaO	TiO_2	Cr_2O_3	FeO	MnO	Total	H_2O	Li	Mg#
MER_10_2	0.33	52.1	15.7	1.51	0.01	19.5	0.36	0.033	9.33	0.733	99.6	130	6.0	79.5
MER_09_3	0.33	51.4	15.3	1.81	0.01	20.5	0.39	0.004	8.43	0.619	98.9	80	4.0	80.7
MER_09_1	0.38	52.0	15.4	1.88	0.00	20.2	0.41	0.000	8.91	0.619	99.7	126	4.5	79.8
MER_01_H2	0.32	37.0	11.2	1.95	0.00	27.4	0.38	0.000	7.20	0.521	85.9	72	3.2	78.2
MER_12_1	0.39	51.7	15.2	2.01	0.01	20.4	0.44	0.000	8.68	0.642	99.5	7	4.2	80.0
MER_11_1	0.38	51.2	15.0	2.15	0.00	20.3	0.47	0.000	8.83	0.612	99.0	99	2.7	79.6
MER_23_2	0.37	51.4	15.1	2.16	0.00	21.1	0.44	0.000	8.24	0.519	99.3	80	4.1	80.8
MER_09_2	0.39	51.6	14.9	2.17	0.00	20.5	0.46	0.009	8.82	0.617	99.5	112	4.1	79.6
MER_28_1	0.38	51.2	14.9	2.49	0.00	20.7	0.56	0.055	8.53	0.599	99.4	145	5.5	80.0
MER_01_H1	0.39	50.8	14.9	2.85	0.01	20.3	0.55	0.000	8.87	0.561	99.3	170	4.2	79.4
MER_01_1	0.37	50.5	14.6	2.93	0.00	20.9	0.61	0.012	8.70	0.502	99.1	28	3.9	79.4
MER_23_3	0.38	50.3	14.0	3.70	0.00	21.7	0.69	0.035	8.79	0.496	100.0	190	1.3	78.5
KAR_35_1	0.03	53.1	23.6	0.75	0.01	1.6	0.31	0.000	19.58	0.935	99.8	6	12.9	73.5
KAR_27_1	0.02	52.8	23.7	0.84	0.00	1.7	0.30	0.000	19.66	0.892	100.0	19	7.7	73.5
KAR_25_2	0.33	51.8	14.7	1.42	0.01	20.7	0.45	0.024	9.68	0.510	99.6	13	18.0	77.7
KAR_25_1	0.33	51.8	14.6	1.44	0.02	20.3	0.55	0.000	10.29	0.494	99.8	11	19.4	76.5
KAR_36_3	0.31	51.5	14.8	1.50	0.01	20.1	0.55	0.000	9.58	0.459	98.9	2	27.0	78.1
KAR_26_1	0.32	51.4	15.1	1.63	0.02	20.1	0.47	0.000	9.36	0.411	98.9	17	44.4	78.8
KAR_17_1	0.34	51.2	14.6	1.86	0.01	19.4	0.62	0.003	10.67	0.409	99.1	9	39.0	75.9
KAR_23_1	0.30	51.7	15.3	1.90	0.00	20.8	0.53	0.000	8.56	0.327	99.4	15	52.2	80.4
KAR_36_1	0.31	51.3	15.0	2.33	0.00	20.1	0.60	0.036	9.40	0.352	99.4	4	45.0	78.6
SSH_13_2	0.03	52.8	23.5	1.17	0.00	1.3	0.22	0.016	20.09	0.783	99.9	122	1.2	72.9
SSH_13_1	0.04	52.3	23.7	1.29	0.00	1.4	0.24	0.000	19.46	0.807	99.2	89	0.8	73.7
SSH_49_1	0.02	52.7	23.5	1.32	0.00	1.3	0.25	0.012	19.93	0.738	99.7	93	1.0	73.0
SSH_49_2	0.03	52.8	23.9	1.40	0.00	1.4	0.25	0.034	19.48	0.686	99.9	129	1.1	73.8
SSH_05	0.31	51.7	13.9	1.56	0.01	20.5	0.26	0.000	10.48	0.543	99.3	90	2.1	75.3
SSH_31_1	0.26	51.3	14.5	1.72	0.01	20.1	0.46	0.000	10.05	0.448	98.8	87	1.7	76.9
SSH_29_1	0.33	51.5	14.2	2.06	0.00	20.4	0.43	0.000	10.34	0.385	99.8	76	1.7	76.0
SSH_02_1	0.32	51.3	15.5	2.39	0.00	19.5	0.64	0.000	9.51	0.285	99.4	140	2.6	78.9
SSH_15_1	0.28	51.4	14.9	2.58	0.00	20.7	0.45	0.000	9.16	0.354	99.8	159	1.5	78.8
SSH_04	0.32	50.8	15.2	2.97	0.00	19.5	0.68	0.009	9.68	0.260	99.5	83	0.9	78.3

Table 2

Click here to download Table: Tab2_MIdata.docx

	Na_2O	SiO_2	MgO	Al_2O_3	K_2O	CaO	Cl	TiO_2	FeO	NiO	MnO	Total	H_2O	Li	B
MER_01_MI1	3.91	63.7	3.29	13.5	4.63	5.45	0.265	0.44	4.67	0.018	0.337	100.5	0.10	10.0	0.6
MER_10_MI4	3.82	65.4	2.28	14.3	5.08	4.02	0.282	0.41	3.30	0.018	0.197	99.4	0.30	14.1	42.6
MER_15_MI1	4.04	62.6	0.43	15.1	4.71	1.36	0.278	0.43	2.61	0.004	0.089	91.7	3.13	33.6	53.9
MER_12_MI2	4.41	68.2	0.35	15.4	5.85	1.02	0.302	0.40	2.45	0.000	0.076	98.7	1.66	41.1	57.6
MER_09_MI4	4.41	67.7	0.34	15.5	5.81	1.07	0.320	0.43	2.52	0.007	0.132	98.2	1.67	43.0	53.0
MER_10_MI3	4.64	66.5	0.52	15.8	5.87	1.55	0.347	0.47	3.14	0.000	0.165	99.2	0.36	31.4	50.2
MER_10_MI7	2.21	66.9	1.21	15.9	4.74	3.32	0.299	0.40	2.94	0.051	0.120	98.2	1.70	42.4	54.8
MER_12_MI1	4.48	67.2	0.37	16.0	5.75	1.11	0.306	0.39	2.53	0.008	0.139	98.5	2.29	44.7	57.2
MER_10_MI6	4.36	67.0	0.64	16.1	5.90	1.35	0.326	0.36	2.72	0.028	0.140	99.0	0.80	38.7	51.2
MER_23_MI1	4.44	67.2	0.48	16.3	5.21	1.39	0.346	0.44	2.66	0.000	0.162	98.9	2.21	37.0	56.1
MER_10_MI2	4.17	67.4	0.39	16.5	5.94	1.21	0.326	0.43	2.69	0.000	0.124	99.4	1.85	44.3	53.2
MER_10_MI1	4.23	67.2	0.39	16.5	5.86	1.23	0.349	0.44	2.71	0.009	0.126	99.3	1.60	40.5	53.6
MER_09_MI3	4.55	66.3	0.54	16.6	5.20	1.21	0.381	0.45	2.75	0.000	0.110	98.4	3.15	56.0	58.4
MER_10_MI5	4.55	66.5	0.18	17.7	4.87	1.87	0.357	0.58	1.66	0.003	0.035	98.4	1.30	43.3	53.4
KAR_42_mat1	4.00	72.4	0.54	12.7	2.90	1.76	0.152	0.99	4.73	0.008	0.156	100.6	0.01	3.2	5.2
KAR_42_mat2	4.39	71.1	0.43	14.2	2.65	2.41	0.137	0.87	4.22	0.039	0.133	100.6	0.02	5.2	6.1
KAR_27_MI1	2.22	69.1	0.59	14.2	2.78	2.99	0.205	0.95	6.20	0.000	0.248	99.6	0.03	3.7	0.3
KAR_25_MI2	4.24	69.7	0.68	14.3	2.40	2.30	0.193	0.68	3.83	0.028	0.171	98.6	2.09	22.4	21.2
KAR_25_MI1	4.24	69.9	0.59	14.7	2.33	2.29	0.217	0.78	3.39	0.000	0.120	98.7	2.47	18.6	22.0
KAR_26_MI1	4.03	67.8	1.06	14.8	2.44	2.58	0.203	0.85	4.06	0.020	0.135	98.1	2.63	18.2	22.6
KAR_36_MI1	4.29	68.5	0.87	15.1	2.50	2.23	0.222	0.97	3.77	0.025	0.105	98.9	2.62	17.4	22.7
KAR_17_MI1	4.03	68.6	0.65	15.5	2.37	2.65	0.190	1.01	3.41	0.027	0.061	98.5	2.40	20.1	25.1
KAR_23_MI1	6.33	67.9	0.56	15.7	2.30	1.57	0.248	0.99	3.38	0.000	0.077	99.4	0.65	6.6	22.8
KAR_36_MI2	3.69	68.9	0.62	16.4	2.23	2.37	0.232	0.91	2.59	0.001	0.099	98.3	2.29	15.9	19.4
SSH_49_MI2	4.30	62.8	4.13	13.2	0.59	8.16	0.057	0.67	5.33	0.006	0.156	99.4	1.04	13.4	4.0
SSH_29_MI1	2.13	58.7	2.36	15.0	2.22	5.70	0.250	0.68	5.57	0.000	0.181	92.9	5.62	24.8	12.3
SSH_05_MI1	4.91	72.6	0.44	16.3	2.61	1.97	0.361	0.22	0.50	0.001	0.127	100.2	1.50	31.5	12.0
SSH_13_MI1	4.08	64.6	0.87	16.4	1.05	4.53	0.326	0.85	3.98	0.007	0.219	97.0	5.06	13.0	11.1
SSH_13_MI2	4.32	63.6	0.78	16.5	0.97	4.24	0.285	0.59	3.44	0.008	0.194	95.0	5.08	13.2	11.3
SSH_49_MI1b	4.49	67.2	0.01	16.9	1.60	3.31	0.356	0.70	0.46	0.011	0.051	95.1	5.48	19.5	15.3
SSH_49_MI1a	4.51	67.6	0.02	17.0	1.58	3.14	0.345	0.48	0.48	0.014	0.060	95.4	6.19	21.0	15.3

Table 3

Click here to download Table: Tab3_Ddata.docx

	Pyr Mg#	Pyr Al_2O_3	Pyr H_2O	Pyr Li, ppm	M.I. H_2O	M.I. Li, ppm	$D_{Li, pyr-melt}$
MER_09_1	79.8	1.88	126	4.5	0.01	10.1	0.45
MER_12_1	80.0	2.01	105	4.2	2.29	44.7	0.09
MER_11_1	79.6	2.15	99	2.7	0.02	6.4	0.42
MER_09_2	79.6	2.17	112	4.1	0.02	10.5	0.39
MER_01_1	79.4	2.93	28	3.9	0.01	6.4	0.62
KAR_35_1	73.5	0.75	13	2.3	0.12	19.5	0.12
KAR_27_1	73.5	0.84	8	2.0	0.03	3.7	0.54
KAR_25_1	76.5	1.44	19	2.1	2.47	18.6	0.11
KAR_26_1	78.8	1.63	44	1.7	2.63	18.2	0.09
KAR_17_1	75.9	1.86	39	2.2	2.40	20.1	0.11
KAR_23_1	80.4	1.90	52	3.4	0.65	6.6	0.51
KAR_36_1	78.6	2.33	45	1.8	2.62	17.4	0.10
SSH_13_1	73.7	1.29	89	0.8	5.06	13.0	0.06
SSH_49_1	73.0	1.32	93	1.0	5.48	19.5	0.05
SSH_49_2	73.8	1.40	129	1.1	6.19	21.0	0.05
SSH_31_1	76.9	1.72	87	1.7	0.01	6.0	0.29
SSH_15_1	78.8	2.58	159	1.5	4.35	14.5	0.10